

# Quantum Nonlinear Effect in Dissipatively Coupled Optomechanical System

Wen-Quan Yang,<sup>1</sup> Wei Niu,<sup>1</sup> Yong-Hong Ma,<sup>2,\*</sup> and Wen-Zhao Zhang<sup>1,†</sup>

<sup>1</sup>*Department of Physics, Ningbo University, Ningbo 315211, China*

<sup>2</sup>*School of Science, Inner Mongolia University of Science and Technology, Baotou 014010, China*

A full-quantum approach is used to study quantum nonlinear properties of a compound Michelson-Sagnac interferometer optomechanical system. The effective Hamiltonian shows that both dissipative and dispersive couplings possess imaginary- and real-Kerr nonlinearities. And unexpectedly, the nonlinearities caused by the dissipative coupling have non-Hermitian Hamiltonian-like properties. It can protect the quantum nature of the dispersive coupling beyond the traditional dissipation of the system. This protection mechanism allows the system to exhibit strong quantum nonlinear effects in the parameter region of the hyperbolic function  $J^2 = \Delta_c \Delta_e$ . Moreover, we can obtain strong anti-bunching effects whether in strong or weak coupling regimes with the help of the dispersive and dissipative couplings jointly. It may provide a new perspective to experimentally realize and study the strong quantum nonlinear effects.

## I. INTRODUCTION

In cavity optomechanics, the interaction of optical fields with mechanical oscillators provides an excellent research platform for the study of fundamental physics and applications [1–3]. The conventional optomechanical interactions are due to the radiation pressure or gradient forces [4] leading to a dispersive shift of the cavity frequency, which has been employed for optomechanical squeezing of optical mode[5, 6], entanglement between optical and mechanical mode [7, 8] as well as for cooling the mechanical oscillators to the quantum ground state [9, 10], and optomechanical normal-mode splitting [11, 12].

Generally, there are two different forms of coupling including the dispersive coupling [1, 13] and the dissipative coupling [14, 15] in the optomechanical interaction. The dispersive coupling typically occurs in conventional optomechanical systems, in which the displacement of mechanical oscillator results in a shift of the resonant frequency for the optical cavity. While the dissipative coupling characterizes the dependence of the cavity decay rate on the displacement of the mechanical oscillator, which was first proposed theoretically by Elste *et al* [15]. Experimentally, the dissipative coupled system was first implemented in the optical domain with Michelson-Sagnac interferometer (MSI), which can cool a mechanical oscillator from room temperature 293 K to 126 mK [10]. Over the last decade, dissipative coupling has been experimentally achieved in different optomechanical devices, such as a waveguide coupled to a microdisk resonator [14], a monolayer graphene membrane in optical resonator [16], a tapered fiber coupled to a whispering-gallery mode [17, 18], and a photonic crystal cavity [19].

Since the optomechanical interaction is essentially nonlinear [1]), there are many interesting applications based on nonlinear interactions have been demonstrated. For

example, the photon blockade [20–24], Kerr nonlinearity [25, 26] and optomechanical induced transparency [27–30]. Recently, the dissipative coupled optomechanical system has attracted considerable attention because of the unique advantages shown in strong driven classical nonlinear effects, such as cooling the mechanical oscillators in the unresolved sideband regime [15, 31, 32], Electromagnetically induced transparency [12, 33] and the squeezing of the output light [34–36]. So far, the classical nonlinear in dissipative coupling have been relatively well studied, but the quantum nonlinear still needs to be further explored. In order to study the quantum nonlinear properties of dissipative coupled systems, the photon blockade effect is an object of great potential. Recently, there are also some interesting related exciting work on photon blockade in dissipative coupled systems, such as the second-order correlation of the output light [35] and the nonreciprocal photon blockade [37]. Reference [35] has shown that the second-order correlation functions exhibit damped oscillations with the minimal  $g^{(2)}(\tau) > 0.4$ , which manifests the classical nonlinear effects under the linear approximation. In addition, Reference [37] has shown that the dissipation coupling of the hybrid dissipation and dispersion optomechanical system can induce the coupling between the environment and system in the cross-Kerr interaction form which obtained under the full quantum approach. However, the former nonlinear effect is obtained under the quantum linear regime, and the latter makes a single-mode approximation of the environment which is difficult to achieve experimentally. In summary, in conjunction with recent advances in photon nonlinear research for dissipative coupled systems, we find that current nonlinear treatments either in the classical nonlinear regime under the linearized approximation or the approach at full quantum by using some experimentally inaccessible approximations. Thus a reasonable approach to study quantum nonlinear in dissipative coupled system is an evident need.

In this paper we propose a scheme to realize strong quantum nonlinear in the dissipative coupling optomechanical system. This scheme does not require the linearized approximation, but only the approximation con-

\* myh\_dlut@126.com

† zhangwenzhao@nbu.edu.cn

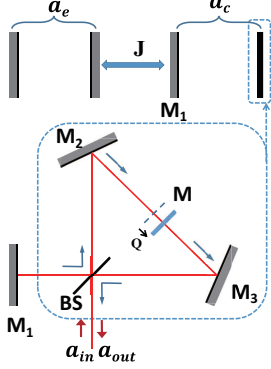


FIG. 1. (color online). The sketch of Michelson-Sagnac interferometer [31] with a movable membrane between the mirror  $M_2$  and  $M_3$  as the effective MSI mirror (the area surrounded by blue dotted line) combined with  $M_1$  into a Fabry-Pérot cavity which coupled to an empty cavity with the tunneling coupling strength  $J$ .

dition of the first order of Taylor expansion and Markov approximation that can be easily achieved in experiments. In our scheme that beyond the linearized approximation, we study the photon blockade effects with the dissipative coupled optomechanical cavity coupled to an empty cavity. Our results show that nonlinear effects in coupled systems must depend on dispersion coupling strength in order to arise. And we also show that the dissipative coupling can induce enhanced nonlinearity, which leads to better photon blockade effects.

The paper is organized as follows. In Sec. II we introduce the system and Hamiltonian. We analysis the second order correlation function in Sec. III. A summary given in Sec. IV.

## II. MODEL AND HAMILTONIAN

A compound MSI optomechanical model [38] that enables both dispersive and dissipative coupling is shown in Fig. 1. Our model contains a standard optical cavity and a MSI optomechanical system which can realize the dispersive and dissipative coupling. In MSI optomechanical system,  $M_1$ ,  $M_2$  and  $M_3$  are perfect total reflection mirrors and the movable membrane  $M$  is a semitransparent membrane. As shown in the diagram, the reflectivity  $R$  and transmissivity  $T$  of the beam splitter (BS) can determine the magnitude of the dispersive coupling  $g_\omega$  [39]. When  $R \neq T$ , a purely dissipative coupled system with  $g_\omega = 0$  can be obtained [31]. The displacement of the membrane can produce dispersive coupling by changing the cavity length i.e.,  $M_1 \rightarrow BS \rightarrow M_2 \rightarrow M$  of the effective cavity. It can also change the optical path difference of the interfering light in the MSI, which is equivalent to change the transmissivity of the effective MSI mirror. When this transmittance changes, the dissipation of the cavity is also modified, and thus the dissipative coupling

arises. The total Hamiltonian of the model is read [15] ( $\hbar = 1$ )

$$\begin{aligned} \hat{H}_T = & \omega_c \hat{a}_c^\dagger \hat{a}_c + \omega_e \hat{a}_e^\dagger \hat{a}_e + \frac{1}{2} \omega_m (\hat{Q}^2 + \hat{P}^2) \quad (1) \\ & + \left[ A \kappa_c \hat{a}_c^\dagger \hat{a}_c + \frac{B}{2} \hat{H}_{int} \right] \hat{Q} + \hat{H}_{int} + \hat{H}_{diss} \\ & + J (\hat{a}_c^\dagger \hat{a}_e + \hat{a}_c \hat{a}_e^\dagger) + \sum_{j=c,e} \epsilon_j (\hat{a}_j^\dagger e^{-i\omega_d t} + h.c.). \end{aligned}$$

The first three terms in Eq. (1) represent the free energy of the optomechanical cavity, empty cavity and the mechanical oscillator, respectively.  $\hat{Q} = \hat{x}/x_{zpf}$  and  $\hat{P} = \hat{p}/(m\omega_m x_{zpf})$  are the dimensionless displacement and momentum operators.  $\hat{x} = x_{zpf}(\hat{b} + \hat{b}^\dagger)$  is the displacement of mechanical oscillator, and  $x_{zpf} = (2m\omega_m)^{-\frac{1}{2}}$  denotes the size of the zero-point fluctuations. The fourth term represents the total cavity-mechanical coupling. Parameters  $A$  and  $B$  denote the weights of the dispersive and dissipative couplings, respectively, and can be derived from the frequency and dissipative shifts. Where the corresponding optical frequency shift per zero-point fluctuation is  $g_\omega = \frac{\partial \omega_c(Q)}{\partial x} x_{zpf} = A \kappa_c$  (dispersive coupling) and dissipation shift per zero-point fluctuation is  $g_\kappa = \frac{\partial \kappa_c(Q)}{\partial x} x_{zpf} = B \kappa_c$  (dissipative coupling). The  $\omega_c(Q)$  and  $\kappa_c(Q)$  denote displacement modified frequency and dissipation, respectively. The fifth term represents the cavity-bath interaction with  $\hat{H}_{int} = i \sqrt{\frac{\kappa_c}{2\pi\rho}} \sum_q (\hat{a}_c^\dagger \hat{b}_q - \hat{b}_q^\dagger \hat{a}_c)$  [40, 41].  $\hat{H}_{diss}$  represent the commonly used bath of the empty-cavity and oscillator as well as the system-bath interactions [42]. The second last term represent the tunneling coupling of optomechanical cavity and empty cavity. The last term denotes the laser driving, which can be introduced by the BS as a semi-classical input to the MSI in our model.

With displacement-modified input-output relation in Markovian regime [31, 42], the Hamiltonian can be reduced by equating the environmental operators  $\sqrt{\frac{\kappa_c}{2\pi\rho}} \sum_q \hat{b}_q$  in the system-environment interaction to  $\sqrt{\kappa_c} \hat{a}_{c,in} - \frac{\kappa_c}{2} \hat{a}_c \left( 1 + \frac{g_\omega}{2\kappa_c} \hat{Q} \right)$  [12]. The corresponding reduced Hamiltonian after eliminate the bath of MSI-cavity and rotating frame operation is then given by [31, 33]

$$\begin{aligned} \hat{H}_R = & -\Delta_c(Q) \hat{a}_c^\dagger \hat{a}_c - \Delta_e \hat{a}_e^\dagger \hat{a}_e + \frac{1}{2} \omega_m (\hat{Q}^2 + \hat{P}^2) \quad (2) \\ & + J (\hat{a}_c^\dagger \hat{a}_e + \hat{a}_c \hat{a}_e^\dagger) + H_{diss} + \sum_{j=c,e} \epsilon_j (\hat{a}_j^\dagger + \hat{a}_j), \end{aligned}$$

where  $\Delta_c(Q) = \omega_d - \omega_c(Q)$  is the displacement-modified detuning.  $\Delta_c = \omega_d - \omega_c$  and  $\Delta_e = \omega_d - \omega_e$  are the driving-detuning of the optomechanical cavity and empty cavity, respectively. Under the first-order approximation (see the Appendix A), we have  $\omega_c(Q) = \omega_c + g_\omega \hat{Q}$  and  $\kappa_c(Q) = \kappa_c + g_\kappa \hat{Q}$ . Where,  $\kappa_c(Q)$  is the displacement-

modified dissipation. Note that, the modified input-output relation  $\hat{a}_{c,out} - \hat{a}_{c,in} = \sqrt{\kappa_c(Q)}\hat{a}_c$  [31, 42] should be considered to investigate the quantum dynamic of the dissipative coupled system. The nonlinear quantum Langevin equations according to Eq. (2) in Markovian regime are given by [43, 44]

$$\dot{\hat{Q}} = \omega_m \hat{P}, \quad (3a)$$

$$\dot{\hat{P}} = -g_\omega \hat{a}_c^\dagger \hat{a}_c - \omega_m \hat{Q} - \frac{ig_\kappa}{2\sqrt{\kappa_c}} (\hat{a}_c^\dagger \hat{a}_{c,in} - \hat{a}_{c,in}^\dagger \hat{a}_c) - \gamma \hat{P} + \hat{\xi}, \quad (3b)$$

$$\dot{\hat{a}}_c = \left[ i(\Delta_c - g_\omega \hat{Q}) - \frac{\kappa_c}{2} (1 + \frac{g_\kappa}{\kappa_c} \hat{Q}) \right] \hat{a}_c - iJ \hat{a}_e + \sqrt{\kappa_c} \left( 1 + \frac{g_\kappa}{2\kappa_c} \hat{Q} \right) \hat{a}_{c,in} + \epsilon_c, \quad (3c)$$

$$\dot{\hat{a}}_e = (i\Delta_e - \frac{\kappa_e}{2}) \hat{a}_e - iJ \hat{a}_c + \sqrt{\kappa_e} \hat{a}_{e,in} + \epsilon_e. \quad (3d)$$

In our discussion, we mainly focus on optical modes. Since the experiment reported decay rate of the mechanical oscillator is much smaller than that of the cavity [1], we can safely use the quantum steady state solution of mechanical mode to solve the optical modes under conditions of long time evolution, in which

$$\dot{\hat{Q}} = \frac{-g_\omega \hat{a}_c^\dagger \hat{a}_c - \frac{ig_\kappa}{2\sqrt{\kappa_c}} (\hat{a}_c^\dagger \hat{a}_{c,in} - \hat{a}_{c,in}^\dagger \hat{a}_c) + \hat{\xi}}{\omega_m}. \quad (4)$$

Bringing Eq. (4) back to Eq. (3c), the mechanical mode can be reduced and thus obtained the dynamical equations for the long-time evolution of the optical modes,

$$\dot{\hat{a}}_c = (i\Delta_c - \frac{\kappa_c}{2}) \hat{a}_c + \frac{2ig_\omega^2 + g_\kappa g_\omega}{2\omega_m} \hat{a}_c^\dagger \hat{a}_c \hat{a}_c - iJ \hat{a}_L + \sqrt{\kappa_c} \hat{\xi}_{eff} + \epsilon_c, \quad (5a)$$

$$\dot{\hat{a}}_e = (i\Delta_e - \frac{\kappa_e}{2}) \hat{a}_e - iJ \hat{a}_c + \sqrt{\kappa_e} \hat{a}_{e,in} + \epsilon_e. \quad (5b)$$

where  $\hat{\xi}_{eff}$  denotes the effective noise operator:

$$\begin{aligned} \hat{\xi}_{eff} = & \frac{ig_\kappa^2 - 2g_\omega g_\kappa}{4\omega_m \kappa_c} (\hat{a}_c^\dagger \hat{a}_{c,in} - \hat{a}_{c,in}^\dagger \hat{a}_c) + \hat{a}_{c,in} \\ & - \frac{ig_\kappa^2}{4\omega_m \kappa_c^{3/2}} (\hat{a}_c^\dagger \hat{a}_{c,in} \hat{a}_{c,in} - \hat{a}_{c,in}^\dagger \hat{a}_{c,in} \hat{a}_c) \\ & + \frac{g_\kappa}{2\omega_m \kappa_c} \hat{\xi} \hat{a}_{c,in} - \frac{(2ig_\omega + g_\kappa)}{2\omega_m \sqrt{\kappa_c}} \hat{\xi} \hat{a}_c \\ & - \frac{g_\kappa g_\omega}{2\omega_m \kappa_c} \hat{a}_c^\dagger \hat{a}_c \hat{a}_{c,in}. \end{aligned} \quad (6)$$

By inverting the dynamical Eqs. (5), the effective Hamil-

tonian is obtained

$$\begin{aligned} \hat{H}_{eff} = & \sum_{j=c,e} \left[ -\Delta_j \hat{a}_j^\dagger \hat{a}_j + \epsilon_j (\hat{a}_j^\dagger + \hat{a}_j) \right] + J(\hat{a}_c^\dagger \hat{a}_e + \hat{a}_c \hat{a}_e^\dagger) \\ & - \frac{(2g_\omega^2 - ig_\kappa g_\omega)}{2\omega_m} \hat{a}_c^\dagger \hat{a}_c \hat{a}_c \hat{a}_c. \end{aligned} \quad (7)$$

This effective Hamiltonian describes the square-coupled nonlinear form of the optical modes in the dissipative coupled system. According to Eq. (7), the nonlinear effect of the system can exist only when the dispersive coupling strength  $g_\omega \neq 0$ . From this particular nonlinear term  $\frac{(2g_\omega^2 - ig_\kappa g_\omega)}{2\omega_m} \hat{a}_c^\dagger \hat{a}_c \hat{a}_c \hat{a}_c$ , it can be seen that in optical modes, dispersive coupling affects both the amplitude and phase of the light (the imaginary and real parts of the nonlinear term), whereas dissipative coupling affects only the amplitude. It is worth noting that this dissipative nonlinear effect is the opposite of the loss effect of the cavity field to the environment. Again, it is visible from the comparison of the sign of  $\frac{\kappa_c}{2} \hat{a}_c$  and  $\frac{g_\kappa g_\omega \hat{N}}{2\omega_m} \hat{a}_c$  in Eqs. (5). This provides us with the possibility that if we choose the suitable strength of the dissipative nonlinearity is able to resist the loss from the environment and thus protect the quantum property of the system. This effect of resisting noise is very similar to the processing of non-Hermitian Hamiltonian [45] and is verified in Fig. 6 of our discussion later.

To characterize the effective Hamiltonian and thus investigate the nonlinear effects of the optical modes in the system more reasonably. We need to analyze the property of the effective noise  $\hat{\xi}_{eff}$  first. In Markov regime, the interaction between the environment and the system is quite weak. Moreover, under the fact that the environment with much larger degrees than the system. Thus, the quantum fluctuations of the environment itself can be neglected when considering the average effect of the environment on the system. In the solution of the Hamiltonian, we can utilize a semi-classical treatment of the effect of the environment as an effective temperature. Especially in the long-time case (steady state), when the system and the environment reach thermal equilibrium, this treatment gives a good description of the behaviour of the thermal environment on the system. All the approximations used in our efficientisation as well as in the later discussion are carried within this premise. The corresponding effective noise is read,

$$\begin{aligned} \hat{\xi}_{eff} \rightarrow & \sqrt{\langle \hat{\xi}_{eff}^\dagger \hat{\xi}_{eff} \rangle} \\ = & \left[ \frac{g_\kappa^4 + 2ig_\omega g_\kappa^3}{16\omega_m^2 \kappa_c^{3/2}} \left( \sqrt{6(\bar{N}^3 - 3\bar{N}^2 + 2\bar{N})} \right. \right. \\ & \left. \left. - \bar{N} \sqrt{\bar{N} - 1} \right) + \frac{4g_\omega^2 g_\kappa^2 + g_\kappa^4}{16\omega_m^2 \kappa_c} (\bar{N}^2 - \bar{N}) \right. \\ & \left. + \frac{(g_\kappa^2 + 4g_\omega^2)}{4\omega_m^2} \bar{N} \bar{n}_{th} \right]^{1/2} / \sqrt{\kappa_c}, \end{aligned} \quad (8)$$

where  $\bar{N} = \langle \hat{a}_c^\dagger \hat{a}_c \rangle$  represent average photon number.  $\bar{n}_{th} = (e^{\omega_m/k_B T_b} - 1)^{-1}$  represent the thermal phonon number of the mechanical oscillator with the Boltzmann constant  $k_B$  and the environmental temperature  $T_b$  of the mechanical oscillator.

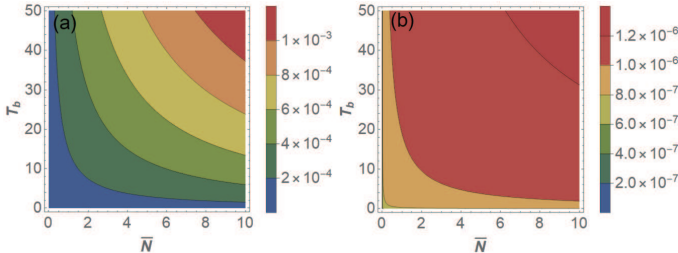


FIG. 2. (Color online) (a) Effective noise as a function of the photon number  $\bar{N}$  and phonon temperature  $T_b(K)$ . (b) Photon temperature  $T_a(K)$  as a function of the photon number  $\bar{N}$  and phonon temperature  $T_b$ . The other parameters are  $\omega_m = 10^6 Hz$ ,  $\kappa = 5 \times 10^3 Hz$ ,  $g_\omega = 200 Hz$ ,  $g_\kappa = 500 Hz$ .

The effective thermal number and effective temperature of the system are illustrated in Fig. 2. As shown in Fig. 2(a), the lower the average photon number and the lower the temperature, we can obtain a lower environmental excitation number. The effective environmental excitation number is almost 4 orders of magnitude smaller than the average photon number. As shown in Fig. 2(b), we can obtain a similar conclusion as in Fig. 2(a). The effective environmental temperature is 7 to 8 orders of magnitude smaller than the real temperature, e.g. when the temperature is 10K and the average photon number is 2, the effective environmental temperature is  $8 \times 10^{-7}$ K. Overall, at the commonly used experimental phonon temperatures [1], the effective environmental temperature is close to zero as long as the driving is weak enough to ensure a low level of average intracavity photon number. In other words, our system has much stronger temperature robustness (effective temperature is 7 orders of magnitude lower than the true temperature).

### III. SECOND ORDER CORRELATION FUNCTION FOR OPTICAL MODE

In our quantum system, the second-order correlation function is a very effective way to evaluate quantum nonlinearity, and its easy to detect in experiment [46]. To investigate the properties of the optical quantum nonlinear effects in dissipative coupled systems, both numerical and analytical methods are used to solve the second-order correlation function for specific analysis. For simplicity, the state truncation method [47] is used to obtain the analytical solution.

In the weak pumping conditions  $C_0 \gg C_{j,ce} \gg C_{jj}, \{j = c, e\}$ . The general optical quantum state in our system after utilising the truncation method is expressed

as,

$$|\psi(t)\rangle = C_0(t)|00\rangle + C_c(t)|10\rangle + C_e(t)|01\rangle + C_{ce}(t)|11\rangle + C_{cc}(t)|20\rangle + C_{ee}(t)|02\rangle, \quad (9)$$

where,  $C_{m,n}$  represent the probability amplitude, and  $|mn\rangle$  represent the photon number state that correspond to OM cavity (c) and empty cavity (e), respectively. Besides, we use second-order correlation function with zero-time delay to represents the statistical properties of photons

$$g_j^{(2)}(0) = \frac{\langle \hat{a}_j^\dagger \hat{a}_j^\dagger \hat{a}_j \hat{a}_j \rangle}{\langle \hat{a}_j^\dagger \hat{a}_j \rangle^2}, \quad j = c, e \quad (10)$$

when  $g^{(2)}(0) < 1$ , the quantum nonlinear effect of the system starts to be visible, and the intracavity photons show an anti-bunching effect, especially when  $g^{(2)}(0) = 0$ , this effect is strongest and photon blockade is achieved. Instead, when  $g^{(2)}(0) > 1$ , the intracavity photons show a bunching effect and the system exhibits classical behaviour. By setting  $\kappa_c = \kappa_e = 0$ , the analytic solution of  $g^{(2)}(0)$  can be obtained as (details see Appendix B)

$$g_c^{(2)}(0) = \left| \frac{2\omega_m K D_J}{f_A} \right|^2, \quad (11a)$$

$$g_e^{(2)}(0) = \left| \frac{D_J [G f_B + 2\omega_m K (J + \Delta_c)^2]}{(J + \Delta_c)^2 f_A} \right|^2, \quad (11b)$$

where  $f_A = (2\omega_m K + G)D_J - G\Delta_e^2$ ,  $f_B = 2J^2 + 2JK + \Delta_c K$  and we define  $D_J = J^2 - \Delta_c \Delta_e$ ,  $K = \Delta_c + \Delta_e$ ,  $G = 2g_\omega^2 - ig_\kappa g_\omega$ . According to Eqs. (11), it is obvious that when  $D_J = 0$ ,  $g_j^{(2)}(0) = 0$ . As seen from the expression of  $D_J = 0$ , when the coupling strength and detuning between the optical cavities satisfy  $J^2 = \Delta_c \Delta_e$ , the photon blockade effect appears. In this case, if  $J$  is fixed,  $g_j^{(2)}(0)$  and  $\Delta_j$  show a hyperbolic relation. For  $g_c^{(2)}(0)$ , in addition to  $D_J = 0$ , the  $K = 0$  also causes  $g_c^{(2)}(0) = 0$ . In this case, we have  $\Delta_c = -\Delta_e$ . For  $g_e^{(2)}(0)$ ,  $K = 0$  does not causes  $g_e^{(2)}(0) = 0$ , whereas when  $J = -\Delta_c$ ,  $g_e^{(2)}(0) \rightarrow \infty$  and the empty cavity exhibits a strong bunching effect. These properties are also shown in Fig. 4 and 5 of the numerical simulations in the following discussion.

To correctly account for the nonlinear effects character of the system, we introduce the quantum master equation [48] for the system density matrix,

$$\begin{aligned} \dot{\rho} = & -i[\hat{H}, \rho] + \sum_{j=c,e} \frac{\kappa_j}{2} \mathcal{D}[\hat{a}_j] \rho + \frac{\gamma}{2} (n_{th} + 1) \mathcal{D}[\hat{b}] \rho \\ & + \frac{\gamma}{2} n_{th} \mathcal{D}[\hat{b}^\dagger] \rho. \end{aligned} \quad (12)$$

$\kappa_j$  and  $\gamma$  are the cavity and mechanical energy decay rates, respectively.  $\mathcal{D}[\hat{o}] \rho = 2\hat{o}\rho\hat{o}^\dagger - \hat{o}^\dagger\hat{o}\rho - \rho\hat{o}^\dagger\hat{o}$  is the Lindblad dissipation superoperator that accounting for

losses to the environment. Then, we will derive the corresponding numerical solutions of Eqs. (11) to analyse the effect of the parameters on the second-order correlation function. The comparison of the analytical and

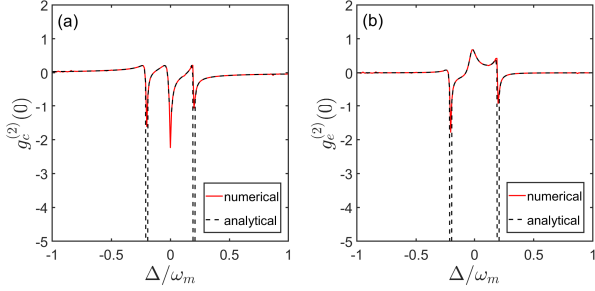


FIG. 3. (Color online) The comparison of the numerical and analytical solutions in the optomechanical cavity (a) and auxiliary cavity (b) with  $\Delta_c = \Delta_e = \Delta$ . The vertical coordinate is zero-time second-order correlation  $\log_{10}g_c^{(2)}(0)$ . The other parameters are  $\omega_m = 10^6 \text{ Hz}$ ,  $\kappa = 5 \times 10^3 \text{ Hz}$ ,  $g_\omega = 200 \text{ Hz}$ ,  $g_\kappa = 500 \text{ Hz}$ ,  $J = 2 \times 10^5 \text{ Hz}$ ,  $\epsilon_c = \epsilon_e = 5 \times 10^3 \text{ Hz}$ .

numerical solutions are shown in Fig. 3. These two solutions are well matched in the figure. In particular, there is a sharp decrease in both the analytic and numerical solutions at  $\Delta/\omega_m = -J/\omega_m = -0.2$ , which represents  $D_J = 0$  (as we have analysed in our analytical solution), i.e.,  $g_c^{(2)}(0) = 0$ . In addition, at this singularity the analytic solution is stronger than the numerical solution in terms of the anti-bunching effect, which is shown in the figure where the black-dashed line is much deeper than the red-solid line. This is because we make  $\kappa = 0$  in analytical solution, so the analytical solution has a better anti-bunching effect. At the value of  $\Delta = 0$ , both the numerical and analytical solutions are very small in Fig. 3(a), which again can be explained in the analytical solution i.e.,  $g_c^{(2)}(0) = 0$  with  $K = 0$ . When  $\Delta_j/\omega_m > 0.2$ , we can see that both numerical and analytical solutions converge to  $g_c^{(2)}(0) = 1$ , which means that the light is in coherent state for the large detuning case. The zero-time second-order correlation of photons in the optomechanical cavity and the empty cavity as a function of the two cavities' detuning are shown in Fig. 4 and 5, respectively. As shown in Fig. 4, the near-photon blockade region (the region surrounded by the white dashed line) matches well with our analyses in the analytical solution: the hyperbolic region and the linear region. For the hyperbolic region, the specific relationship between  $\Delta_c$  and  $\Delta_e$  can be obtained by the analytical solution of Eqs. (11), i.e.,  $\Delta_c = J^2/\Delta_e$ . For the linear region, we can also obtain the relationship  $\Delta_c = -\Delta_e$  by using  $K = 0$  from Eqs. (11). While, when  $\Delta_c$  and  $\Delta_e$  do not satisfy these two conditions,  $g_c^{(2)}(0)$  increases rapidly and the cavity exhibits classical effects. Especially when  $-\Delta_e = J$ , Fig. 4 shows a strong bunching effect. This special condition can be understood from the effective Hamiltonian in Eq. (7), when  $-\Delta_e = J$ ,

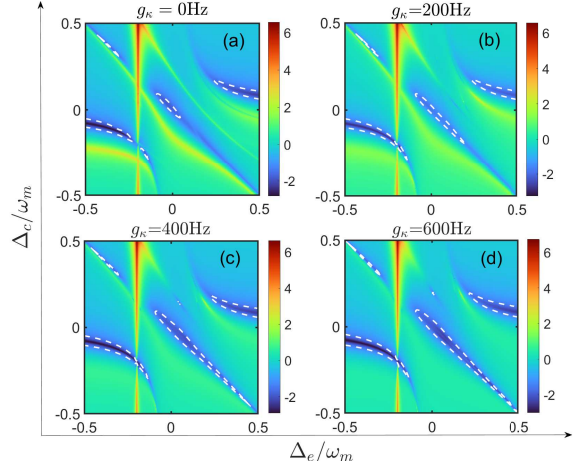


FIG. 4. (Color online) Zero-time second-order correlation  $g_c^{(2)}(0)$  as a function of the detuning  $\Delta_c/\omega_m$  and  $\Delta_e/\omega_m$  in optomechanical cavity. Where  $g_\omega = 400 \text{ Hz}$  does not change and  $g_\kappa$  is 0, 200, 400 and 600 Hz respectively. The white dotted line represents the value of  $\log_{10}[g_c^{(2)}(0)] = -1.5$ . The other parameters are  $\omega_m = 10^6 \text{ Hz}$ ,  $\kappa = 5 \times 10^3 \text{ Hz}$ ,  $J = 2 \times 10^5 \text{ Hz}$ ,  $\epsilon_c = \epsilon_e = 5 \times 10^3 \text{ Hz}$ .

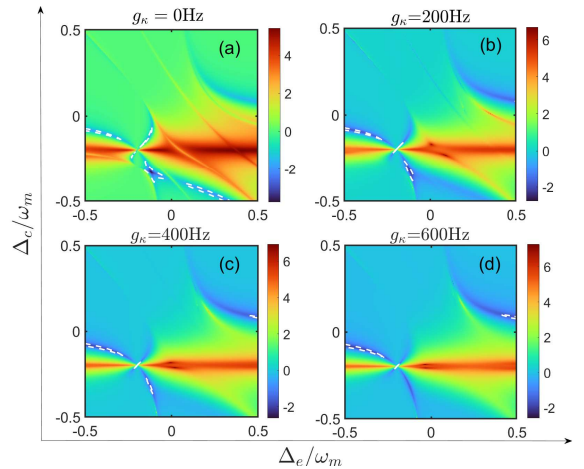


FIG. 5. (Color online) Zero-time second-order correlation  $g_c^{(2)}(0)$  as a function of the detuning  $\Delta_c/\omega_m$  and  $\Delta_e/\omega_m$  in empty cavity. Where  $g_\omega = 400 \text{ Hz}$  does not change and  $g_\kappa$  is 0, 200, 400 and 600 Hz, respectively. The white dotted line represents the value of  $\log_{10}[g_c^{(2)}(0)] = -1.5$ . The other parameters are  $\omega_m = 10^6 \text{ Hz}$ ,  $\kappa = 5 \times 10^3 \text{ Hz}$ ,  $J = 2 \times 10^5 \text{ Hz}$ ,  $\epsilon_c = \epsilon_e = 5 \times 10^3 \text{ Hz}$ .

the detuning energy of the empty-cavity is exactly the same as the energy of the BS interaction. Therefore, the energy of the empty-cavity can be converted into the OM-cavity through a resonance-like effect. Due to the condition  $J \gg \{g_\kappa, g_\omega\}$ , the converted energy can eliminate the blockade effect due to nonlinear energy shift ( $\propto n^2$ ) and excite the photons in the OM-cavity, thus to exhibit a bunching effect. Comparing four plots, it shows that  $g_\kappa$  has an optimising effect on  $g_c^{(2)}(0)$ . Although the increase of  $g_\kappa$  does not result a significant

decrease of  $g_c^{(2)}(0)$ , it does increase the range of parameters in the near-photon blockade region. That is because as the  $g_\kappa$  increasing, the  $|G|$  is also increasing. In addition, due to  $g_c^{(2)}(0) \propto \frac{1}{|(D_J - \Delta_e^2)G + 2\omega_m K D_J|^2}$ , as  $|G|$  increases,  $g_c^{(2)}(0)$  is decreasing. This increase is more visible in the comparison in Fig. 4(a), (b), (c), and this increasing trend is relatively saturated when  $g_\kappa$  exceeds 400Hz. A similar conclusions can be obtained in the empty-cavity, as shown in Fig. 5, where the region of the minimum value of the second-order correlation function (the blue region in the figure) exhibits a clear hyperbolic function characteristic. Differently, in Fig. 5, the near-photon blockade region is gradually becoming smaller as  $g_\kappa$  increases, which is the opposite of Fig. 4. While  $g_e^{(2)}(0) \propto \left| \frac{D_J f_B G + X}{(J + \Delta_c)^2 (D_J - \Delta_e^2) G + Y} \right|^2$  ( $X$  and  $Y$  are constant), and  $|D_J f_B| > |(J + \Delta_c)^2 (D_J - \Delta_e^2)|$ , thus as  $g_\kappa$  increases, so does  $g_e^{(2)}(0)$ . Thus,  $g_\kappa$  has a negative damping of the photon blockade effect in the empty cavity.

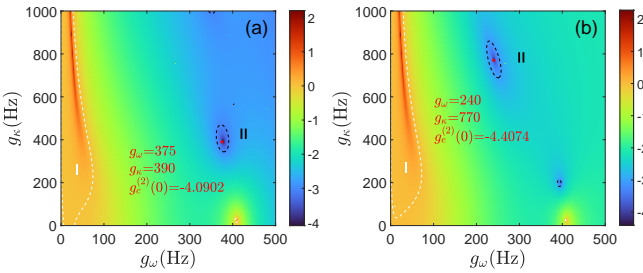


FIG. 6. (Color online) Zero-time second-order correlation  $g^{(2)}(0)$  as a function of the dispersive coupling strength  $g_\omega$  and dissipative coupling strength  $g_\kappa$  in optomechanical cavity (a) and empty cavity (b). The blank dotted line represents the value of  $\log_{10}[g^{(2)}(0)] = -3$ , the white dotted line represents the value of  $\log_{10}[g^{(2)}(0)] = 0$ , and the red point represent the minimum of the  $g^{(2)}(0)$  (It's size and coordinate is also shown in the figure). The other parameters are  $\omega_m = 10^6 Hz$ ,  $\kappa = 5 \times 10^3 Hz$ ,  $\Delta_c = \Delta_e = -2 \times 10^5 Hz$ ,  $J = 2 \times 10^5 Hz$ ,  $\epsilon_c = \epsilon_e = 5 \times 10^3 Hz$ .

Besides the effect of detuning on the system, we still need to explore the contribution of dissipative and dispersive coupling to the second-order correlation function. We select the detuning parameters of the near-blockade region in Fig. 4 and 5 with  $\Delta_c = \Delta_e = -J$  to investigate this contribution and illustrate in Fig. 6. As shown in Fig. 6, for the second-order correlation function,  $g_\omega$  and  $g_\kappa$  exhibit a complex nonlinear relationship for both the OM- and empty-cavities. For the  $g_c^{(2)}(0)$  of OM-cavity shown in Fig. 6(a), overall, when  $g_\omega$  is small, large  $g_\kappa$  is needed to obtain photon blockade effect. We have also marked the  $\log_{10}[g^{(2)}(0)] \geq 0$  region (I-region) in the figure to demonstrate this result clearly. Region II with  $\log_{10}[g^{(2)}(0)] \leq -3$  are also marked in the figure to observe the optimal  $g_c^{(2)}(0)$ . This region can exhibit strong parameter dependencies, with the optimal point

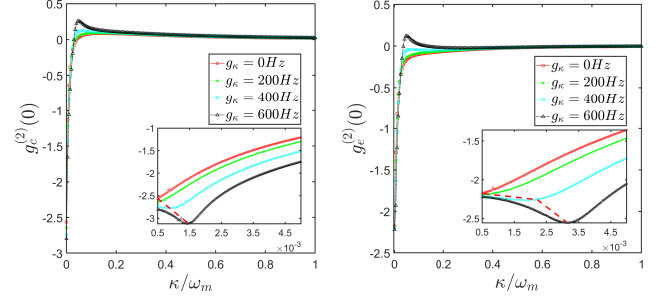


FIG. 7. (Color online) Zero-time second-order correlation  $g^{(2)}(0)$  as a function of the dissipation  $\kappa/\omega_m$  in two cavities. Where  $g_\omega = 200 Hz$  does not change and  $g_\kappa$  is 0, 200, 400 and 600 Hz, respectively. The other parameters are  $\omega_m = 10^6 Hz$ ,  $\Delta_c = \Delta_e = -J = -2 \times 10^5 Hz$ ,  $\epsilon_c = \epsilon_e = 5 \times 10^3 Hz$ .

arising when both  $g_\omega$  and  $g_\kappa$  are at specific values. Compared with the case without dissipative coupling (which is shown in the region of  $g_\kappa = 0$  in the figure), an improved photon blockade is obtained with the help of dissipative coupling. Similar to Fig. 6(a) the results can also be obtained in the empty-cavity shows in Fig. 6(b). Note that a better blockade effect can be obtained in Fig. 6(b), even the nonlinear effects in the empty-cavity arise from the OM-cavity. This conclusion also corresponds to the trend in Fig. 3, i.e., the minimum value of the numerical solution in (b) is smaller than the minimum value in (a) at  $\Delta = -J$  in Fig. 3.

In addition, the impact of dissipation on the system is shown in Fig. 7. The second-order correlation function appears to be a minimum as  $\kappa$  increases and that the minimal value decreases as the dissipative coupling strength  $g_\kappa$  increases. The red dotted line in the graph represents the moving trend of the minimum value. As  $\kappa$  increases, the location of this minimum value gradually shifts to the right. This phenomenon can be explained by Eq. (5). When the dissipative coupling term  $g_\kappa g_\omega / 2\omega_m \hat{a}_c^\dagger \hat{a}_c \hat{a}_c$  is equal to the optical dissipative term  $\kappa_c / 2\hat{a}_c$ , the system can be treated as a dissipation-free system, and the nonlinear effect of the system is well demonstrated, thus minimal value arise. This process is similar to the inverse dissipation in non-Hermitian Hamiltonian and is discussed in the analysis of Eq. (7). The corresponding relationship for the  $\kappa$  at the minimum second-order correlation function is derived as  $\kappa_{min} \propto \frac{g_\kappa g_\omega}{2\omega_m}$ . Thus, as the product of  $g_\kappa g_\omega$  becomes larger,  $\kappa_{min}$  increases gradually.

In the previous analysis  $J$  is also a very important parameter which can be tuned in waveguide-coupled and close-coupled optical systems [49, 50]. As shown in Fig. 8, the effect of  $J$  and the detuning on the second-order correlation function is analysed. In the figure we have taken the detuning at the resonance point, i.e.  $\Delta_c = \Delta_e = \Delta$ . The photon blockade effect (black-dashed line) only occurs when  $J = -\Delta$  and the second-order correlation function increases rapidly when  $J \neq -\Delta$ . At  $\Delta = 0$ , figure (a) shows anti-bunching effect while figure (b) shows bunching effect (white-dashed line). This difference can

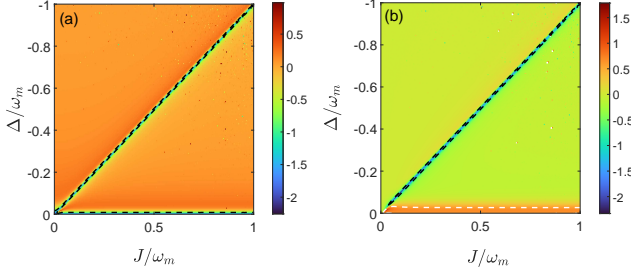


FIG. 8. (Color online) Zero-time second-order correlation  $g^{(2)}(0)$  as a function of the cavity coupling strength  $J$  and detuning  $\Delta$  in optomechanical cavity (a) and auxiliary cavity (b). The black dashed line represents  $\log_{10}[g^{(2)}(0)] = -1$  and the white dashed line represents  $\log_{10}[g^{(2)}(0)] = 0.602$ . The other parameters are  $\omega_m = 10^6 \text{ Hz}$ ,  $\kappa = 5 \times 10^3 \text{ Hz}$ ,  $\Delta_c = \Delta_e = \Delta$ ,  $g_\omega = 200 \text{ Hz}$ ,  $g_\kappa = 500 \text{ Hz}$ ,  $\epsilon_c = \epsilon_e = 5 \times 10^3 \text{ Hz}$ .

be understood by the analytical solution. In Eq. (11a), at  $\Delta = 0$ ,  $g_c^{(2)}(0) = 0$ . In Eq. (11b), at  $\Delta = 0$ ,  $g_e^{(2)}(0) = 4$ .

#### IV. DISCUSSION AND CONCLUSION

In our discussion, we have chosen the eigenfrequency of the mechanical oscillator in the order of  $10^6 \text{ Hz}$ , which is the commonly used frequency for suspended mirrors in experiments for optomechanical systems [1, 51, 52]. This is also close to the experimentally reported frequency of SiN membrane in the MSI-based dissipative coupled systems with  $\omega_m = 2\pi \times 136 \text{ kHz}$  [10]. Note that we don't have any special requirements for the selection of this frequency. The detailed discussion in Fig. 7 shows that we can obtain  $g_j^{(2)}(0) < 10^{-1}$  with  $\kappa/\omega_m < 10^{-2}$ . And this requirement under resolved sideband has been realised in many optomechanical systems [53–55]. For single-photon coupling rates, it is currently still in the weak coupling regime in experiments [51, 55–57], i.e.  $g/\omega_m \in \{10^{-9} - 10^{-1}\}$ . In Fig. 4 and 5, we show that it is possible to realise strong anti-bunching effect in the weak coupling regime, with required  $g_{\omega(\kappa)}/\omega_m$  in the order  $10^{-4}$  to  $10^{-3}$ . In addition, our system is tolerant to temperature, and the equivalent temperature is reduced by 7 to 8 orders of magnitude through the treatment of the effective process (see Fig. 2), e.g., 10K for the original temperature of  $8 \times 10^{-7} \text{ K}$  after the effective process.

Overall, We first give a full-quantum method to study the dissipative coupled system without linearized approximation. A strong anti-bunching effect is discovered in nonlinear and linear parameters region of the driving detunings in weak coupling regime. The optimal region of second-order correlation function is a hyperbolic form with relationship  $J^2 = \Delta_c \Delta_e$ .  $g_\omega$  and  $g_\kappa$  exhibit strong interconnection properties for the quantum nonlinear effects of the system. When they satisfy specific conditions (as shown in Fig. 6), the system exhibit photon blockade effect. In addition, a special effect of the dissipative cou-

pling is discovered: its ability to resist the destruction of the quantum effects by conventional dissipation (as shown in Fig. 7).

In our discussion, we confirm the validity of the dissipative coupling theory in the study of quantum nonlinear effects in optomechanical systems. The quantum nonlinear effects due to the protective effect of dissipative coupling require neither strong single-photon coupling coefficients as in conventional blockade [20, 58, 59] nor stringent parametrics condition as in unconventional blockade [60–63]. This dissipative coupling-assisted blockade effect is of great benefit for performing single-photon transmission control [48] and implementing optical quantum diodes [64, 65]. In quantum information processing, MSI-based optomechanical systems can also serve as a core to realize optical and mechanical-optical controlled gates [66–68]. Moreover, this strong nonlinearity is a necessary resource in quantum synchronization [69–72] and the study of quantum chaos effects [73]. Also, MSI serves as a kindly platform for exploring classical and quantum transitions in the nonlinear regime [74, 75] due to the advantage of the quantized mechanical oscillator for studying classical quantum boundary [76, 77].

#### V. ACKNOWLEDGMENTS

We appreciate Qiu Hui-Hui, Rui-Jie Xiao and Leng Xuan's constructive discussions. This work was partly supported by the National Natural Science Foundation of China under Grant Nos. 12074206 and 12265022, the Natural Science Foundation of Zhejiang Province under Grant No. LY22A040005, the Inner Mongolia Natural Science Foundation under Grant No. 2021MS01012 and K. C. Wong Magna Fund in Ningbo University.

#### Appendix A: Approximate derivation of dissipative coupling

The dependence of the cavity decay rate  $\kappa_c(L + \hat{x})$  on the displacement of the mechanical oscillator  $\hat{x}$ . Since the displacement of the mechanical oscillator is very small compared to the cavity length, a Taylor expansion can be made for  $\kappa_c(L + \hat{x})$ :

$$\kappa_c(L + \hat{x}) = \kappa_c(L) + \frac{\partial \kappa_c(L)}{\partial L} \hat{x} + \frac{\partial^2 \kappa_c(L)}{2\partial^2 L} \hat{x}^2 + o\left(\frac{\hat{x}}{L}\right)^3, \quad (\text{A1})$$

With a movable ideal end mirror and an input coupler of transmissivity  $\tau$ , the cavity linewidth  $\kappa_c$  is given by [31]

$$\kappa_c(L + \hat{x}) = \frac{c|\tau|^2}{4(L + \hat{x})}, \quad (\text{A2})$$

Substituting back to Eq. A1 and ignoring the higher order terms, we can approximate to the first order term

$$\kappa_c(L + \hat{x}) = \frac{c|\tau^2|}{4L}(1 - \frac{\hat{x}}{L}), \quad (\text{A3})$$

We define  $\kappa_c = \kappa_c(L) = \frac{c|\tau^2|}{4L}$ ,  $g_\kappa = \frac{\partial \kappa_c(L)}{\partial L} x_{zpf} = -\frac{\kappa_c}{L} x_{zpf}$ . Thus we get  $L = -\frac{\kappa_c}{g_\kappa} x_{zpf}$  and the square root form with  $\hat{x} = \hat{Q} x_{zpf}$ :

$$\begin{aligned} \sqrt{\kappa_c(L + \hat{x})} &= \sqrt{\kappa_c + g_\kappa \hat{Q}} = \sqrt{\frac{c|\tau^2|}{4L}(1 - \frac{\hat{x}}{L})} \\ &\approx \sqrt{\kappa_c}(1 - \frac{\hat{x}}{2L}) = \sqrt{\kappa_c}(1 + \frac{g_\kappa}{2\kappa_c} \hat{Q}). \end{aligned} \quad (\text{A4})$$

## Appendix B: Derivation of second order correlation function

With the definition  $D_J = J^2 - \Delta_c \Delta_e$ ,  $K = \Delta_c + \Delta_e$ ,  $G = 2g_\omega^2 - ig_\kappa g_\omega$  and set  $\kappa_c = \kappa_e = 0$ ,  $\epsilon_c = \epsilon_e = \epsilon$  under the weak-driving condition ( $C_0 \gg C_m \gg C_{mn}$ ), we can obtain the dynamic equations of the probability amplitudes.

$$\begin{aligned} i\dot{C}_c &= \epsilon_c C_0 + J C_e - \Delta_c C_c, \\ i\dot{C}_e &= \epsilon_e C_0 + J C_c - \Delta_e C_e, \\ i\dot{C}_{ce} &= \epsilon_e C_c + \epsilon_c C_e + \sqrt{2}J(C_{ee} + C_{cc}) - K C_{ce}, \\ i\dot{C}_{cc} &= \sqrt{2}\epsilon_c C_c + \sqrt{2}J C_{ce} - 2(\Delta_c + \frac{G}{2\omega_m}) C_{cc}, \\ i\dot{C}_{ee} &= \sqrt{2}\epsilon_e C_e + \sqrt{2}J C_{ce} - 2\Delta_e C_{ee}. \end{aligned} \quad (\text{B1})$$

The corresponding steady-state solutions are obtained as

$$\begin{aligned} C_c &= C_e = -\frac{\epsilon(J + \Delta_e)}{D_J}, \\ C_{ce} &= \epsilon^2 \frac{[G(J + K) + 2K\omega_m(J + \Delta_e)](J + \Delta_e)}{D_J[2KD_J\omega_m + G(J^2 - K\Delta_e)]}, \\ C_{cc} &= \frac{\sqrt{2}K\epsilon^2\omega_m(J + \Delta_e)^2}{D_J[2KD_J\omega_m + G(J^2 - K\Delta_e)]}, \\ C_{ee} &= \epsilon^2 \frac{G[2J(J + K) + K\Delta_e] + 2K\omega_m(J + \Delta_e)^2}{\sqrt{2}D_J[2KD_J\omega_m + G(J^2 - K\Delta_e)]}. \end{aligned} \quad (\text{B2})$$

Thus, the second-order correlation functions with zero time delay are read:

$$\begin{aligned} g^{(2)}(0) &= \frac{\sum_{n=1}^2 n(n-1)P(n)}{[\sum_{n=1}^2 nP(n)]^2}, \\ g_c^{(2)}(0) &= \frac{2|C_{cc}^2|}{(|C_c|^2 + |C_{ce}|^2 + 2|C_{cc}|^2)^2} \approx \frac{2|C_{cc}|^2}{|C_c|^4}, \\ g_e^{(2)}(0) &= \frac{2|C_{ee}^2|}{(|C_e|^2 + |C_{ce}|^2 + 2|C_{ee}|^2)^2} \approx \frac{2|C_{ee}|^2}{|C_e|^4}. \end{aligned} \quad (\text{B3})$$

---

[1] M. Aspelmeyer, T. J. Kippenberg, and F. Marquardt, *Rev. Mod. Phys.* **86**, 1391 (2014).

[2] T. Kippenberg and K. Vahala, *Opt. Express* **15**, 17172 (2007).

[3] T. J. Kippenberg and K. J. Vahala, *Science* **321**, 1172 (2008).

[4] T. Faust, P. Krenn, S. Manus, J. P. Kotthaus, and E. M. Weig, *Nature communications* **3**, 728 (2012).

[5] T. P. Purdy, P.-L. Yu, R. W. Peterson, N. S. Kampel, and C. A. Regal, *Phys. Rev. X* **3**, 031012 (2013).

[6] R. Schnabel, *Physics Reports* **684**, 1 (2017), squeezed states of light and their applications in laser interferometers.

[7] M. Paternostro, D. Vitali, S. Gigan, M. S. Kim, C. Brukner, J. Eisert, and M. Aspelmeyer, *Phys. Rev. Lett.* **99**, 250401 (2007).

[8] D.-G. Lai, Y.-H. Chen, W. Qin, A. Miranowicz, and F. Nori, *Phys. Rev. Res.* **4**, 033112 (2022).

[9] M. Bhattacharya and P. Meystre, *Phys. Rev. Lett.* **99**, 073601 (2007).

[10] A. Sawadsky, H. Kaufer, R. M. Nia, S. P. Tarabrin, F. Y. Khalili, K. Hammerer, and R. Schnabel, *Phys. Rev. Lett.* **114**, 043601 (2015).

[11] S. Huang and G. S. Agarwal, *Phys. Rev. A* **81**, 053810 (2010).

[12] T. Weiss, C. Bruder, and A. Nunnenkamp, *New Journal of Physics* **15**, 045017 (2013).

[13] C. K. Law, *Phys. Rev. A* **51**, 2537 (1995).

[14] M. Li, W. H. P. Pernice, and H. X. Tang, *Phys. Rev. Lett.* **103**, 223901 (2009).

[15] F. Elste, S. M. Girvin, and A. A. Clerk, *Phys. Rev. Lett.* **102**, 207209 (2009).

[16] H. M. Meyer, M. Breyer, and M. Köhl, *Applied Physics B* **122**, 1432 (2016).

[17] R. Madugani, Y. . Yang, J. M. Ward, V. H. Le, and S. Nic Chormaic, *Applied Physics Letters* **106**, 241101 (2015).

[18] J.-W. Meng, S.-J. Tang, J. Sun, K. Shen, C. Li, Q. Gong, and Y.-F. Xiao, *Phys. Rev. Lett.* **129**, 073901 (2022).

[19] M. Wu, A. C. Hryciw, C. Healey, D. P. Lake, H. Jayakumar, M. R. Freeman, J. P. Davis, and P. E. Barclay, *Phys. Rev. X* **4**, 021052 (2014).

[20] P. Rabl, *Phys. Rev. Lett.* **107**, 063601 (2011).

[21] A. Nunnenkamp, K. Børkje, and S. M. Girvin, *Phys. Rev. Lett.* **107**, 063602 (2011).

[22] T. C. H. Liew and V. Savona,

*Phys. Rev. Lett.* **104**, 183601 (2010).

[23] A. Miranowicz, M. Paprzycka, Y.-x. Liu, J. c. v. Bajer, and F. Nori, *Phys. Rev. A* **87**, 023809 (2013).

[24] R. Huang, A. Miranowicz, J.-Q. Liao, F. Nori, and H. Jing, *Phys. Rev. Lett.* **121**, 153601 (2018).

[25] S. Aldana, C. Bruder, and A. Nunnenkamp, *Phys. Rev. A* **88**, 043826 (2013).

[26] L. Zhou, J. Cheng, Y. Han, and W. Zhang, *Phys. Rev. A* **88**, 063854 (2013).

[27] S. Weis, R. Rivière, S. Deléglise, E. Gavartin, O. Arcizet, A. Schliesser, and T. J. Kippenberg, *Science* **330**, 1520 (2010).

[28] A. Kronwald and F. Marquardt, *Phys. Rev. Lett.* **111**, 133601 (2013).

[29] G. S. Agarwal and S. Huang, *Phys. Rev. A* **81**, 041803 (2010).

[30] J. D. Teufel, D. Li, M. Allman, K. Cicak, A. Sirois, J. Whittaker, and R. Simmonds, *Nature* **471**, 204 (2011).

[31] A. Xuereb, R. Schnabel, and K. Hammerer, *Phys. Rev. Lett.* **107**, 213604 (2011).

[32] A. K. Tagantsev, *Phys. Rev. A* **102**, 043520 (2020).

[33] S. Huang, L. Deng, and A. Chen, *Phys. Rev. A* **107**, 013524 (2023).

[34] K. Qu and G. S. Agarwal, *Phys. Rev. A* **91**, 063815 (2015).

[35] D. Kilda and A. Nunnenkamp, *Journal of Optics* **18**, 014007 (2015).

[36] A. K. Tagantsev, I. V. Sokolov, and E. S. Polzik, *Phys. Rev. A* **97**, 063820 (2018).

[37] Y.-P. Gao and C. Wang, *Opt. Express* **29**, 25161 (2021).

[38] K. Yamamoto, D. Friedrich, T. Westphal, S. Gofbler, K. Danzmann, K. Somiya, S. L. Danilishin, and R. Schnabel, *Phys. Rev. A* **81**, 033849 (2010).

[39] S. P. Tarabrin, H. Kaufer, F. Y. Khalili, R. Schnabel, and K. Hammerer, *Phys. Rev. A* **88**, 023809 (2013).

[40] P. Zoller and C. W. Gardiner, “Quantum noise in quantum optics: the stochastic schrödinger equation,” (1997), arXiv:quant-ph/9702030 [quant-ph].

[41] A. A. Clerk, M. H. Devoret, S. M. Girvin, F. Marquardt, and R. J. Schoelkopf, *Rev. Mod. Phys.* **82**, 1155 (2010).

[42] C. W. Gardiner and M. J. Collett, *Phys. Rev. A* **31**, 3761 (1985).

[43] Q. He, F. Badshah, Y. Song, L. Wang, E. Liang, and S.-L. Su, *Phys. Rev. A* **105**, 013503 (2022).

[44] A. Mehmood, S. Qamar, and S. Qamar, *Physica Scripta* **95**, 035102 (2020).

[45] X. Z. Hao, X. Y. Zhang, Y. H. Zhou, W. Li, S. C. Hou, and X. X. Yi, *Phys. Rev. A* **103**, 053508 (2021).

[46] O. Arcizet, V. Jacques, a. Siria, P. Poncharal, P. Vincent, and S. Seidelin, *Nature Physics* **7**, 879 (2011).

[47] M. Bamba, A. Imamoglu, I. Carusotto, and C. Ciuti, *Phys. Rev. A* **83**, 021802 (2011).

[48] W.-Z. Zhang, J. Cheng, J.-Y. Liu, and L. Zhou, *Phys. Rev. A* **91**, 063836 (2015).

[49] A. H. Safavi-Naeini and O. Painter, *Optics Express* **18**, 14926 (2010).

[50] L. Cai, J. Pan, and S. Hu, *Optics and Lasers in Engineering* **127**, 105968 (2020).

[51] M. Yuan, V. Singh, Y. M. Blanter, and G. A. Steele, *Nature Communications* **6**, 8491 (2015).

[52] O. Arcizet, P.-F. Cohadon, T. Briant, M. Pinard, A. Heidmann, J.-M. Mackowski, C. Michel, L. Pinard, O. Français, and L. Rousseau, *Phys. Rev. Lett.* **97**, 133601 (2006).

[53] J. D. Teufel, T. Donner, D. Li, J. W. Harlow, M. S. Allman, K. Cicak, A. J. Sirois, J. D. Whittaker, K. W. Lehnert, and R. W. Simmonds, *Nature* **475**, 359 (2011).

[54] Y.-S. Park and H. Wang, *Nature Physics* **5**, 489 (2009).

[55] Y. Chen, Y.-L. Zhang, Z. Shen, C.-L. Zou, G.-C. Guo, and C.-H. Dong, *Phys. Rev. Lett.* **126**, 123603 (2021).

[56] J. D. Teufel, D. Li, M. S. Allman, K. Cicak, A. J. Sirois, J. D. Whittaker, and R. W. Simmonds, *Nature* **471**, 204 (2011).

[57] D. W. C. Brooks, T. Botter, S. Schreppler, T. P. Purdy, N. Brahms, and D. M. Stamper-Kurn, *Nature* **488**, 476 (2012).

[58] J.-Q. Liao and F. Nori, *Phys. Rev. A* **88**, 023853 (2013).

[59] K. Hou, C. J. Zhu, Y. P. Yang, and G. S. Agarwal, *Phys. Rev. A* **100**, 063817 (2019).

[60] H. Flayac and V. Savona, *Phys. Rev. A* **96**, 053810 (2017).

[61] M.-A. Lemonde, N. Didier, and A. A. Clerk, *Phys. Rev. A* **90**, 063824 (2014).

[62] B. Sarma and A. K. Sarma, *Phys. Rev. A* **98**, 013826 (2018).

[63] H. Z. Shen, C. Shang, Y. H. Zhou, and X. X. Yi, *Phys. Rev. A* **98**, 023856 (2018).

[64] D.-W. Wang, H.-T. Zhou, M.-J. Guo, J.-X. Zhang, J. Evers, and S.-Y. Zhu, *Phys. Rev. Lett.* **110**, 093901 (2013).

[65] J. C. Blakesley, P. See, A. J. Shields, B. E. Kardynal, P. Atkinson, I. Farrer, and D. A. Ritchie, *Phys. Rev. Lett.* **94**, 067401 (2005).

[66] Q. Lin and J. Li, *Phys. Rev. A* **79**, 022301 (2009).

[67] W.-Z. Zhang, J. Cheng, and L. Zhou, *Journal of Physics B: Atomic, Molecular and Optical Physics* **48**, 015001 (2015).

[68] M. Asjad, P. Tombesi, and D. Vitali, *Optics Express* **23**, 7786 (2015).

[69] A. Mari, A. Farace, N. Didier, V. Giovannetti, and R. Fazio, *Phys. Rev. Lett.* **111**, 103605 (2013).

[70] W. Li, C. Li, and H. Song, *Phys. Rev. E* **95**, 022204 (2017).

[71] S. Walter, A. Nunnenkamp, and C. Bruder, *Phys. Rev. Lett.* **112**, 094102 (2014).

[72] M. Zhang, G. S. Wiederhecker, S. Manipatruni, A. Barnard, P. McEuen, and M. Lipson, *Phys. Rev. Lett.* **109**, 233906 (2012).

[73] X.-Y. Lü, H. Jing, J.-Y. Ma, and Y. Wu, *Phys. Rev. Lett.* **114**, 253601 (2015).

[74] E. B. Rozenbaum, L. A. Bunimovich, and V. Galitski, *Phys. Rev. Lett.* **125**, 014101 (2020).

[75] S. Chaudhury, A. Smith, B. E. Anderson, S. Ghose, and P. S. Jessen, *Nature* **461**, 768 (2009).

[76] F. Fröwis, P. Sekatski, W. Dür, N. Gisin, and N. Sangouard, *Rev. Mod. Phys.* **90**, 025004 (2018).

[77] A. Bassi, K. Lochan, S. Satin, T. P. Singh, and H. Ulbricht, *Rev. Mod. Phys.* **85**, 471 (2013).